Fugitive Dust Source Mapping at a Colton, California Cement Processing Facility Using an Eye-safe U.V. Scanning Lidar

FINAL REPORT
(February 2011)

Prepared for the
South Coast Air Quality Management District
21865 Copley Dr, Diamond Bar, CA 91765

by

S.M. Beck, M.E. Sklar, and J.R. Linares
The Aerospace Corporation
2310 E. El Segundo Blvd.
El Segundo, CA 90245

TABLE OF CONTENTS

EXECUTIVE SUMMARY

Commercial cement production involves a series of steps which can produce significant quantities of fugitive dust emissions that present potential health risks for neighboring areas. It is therefore critical that a detailed account of cement production processes and their contribution to the particulate matter (PM) emission inventory be available to air quality management agencies. In order to address that need, a joint project was initiated between South Coast Air Quality Management District (SCAQMD) and The Aerospace Corporation (Aerospace). The goal of the project was to assess the feasibility of using Light Detection and Ranging (LIDAR) technology for detailed mapping of dust emission sources at a cement production facility located in Colton, California. Lidar is a remote sensing technique which involves mapping the presence of dust in the air from the back-scattered light it produces when illuminated by laser light. It is capable of producing a three dimensional map of dust clouds. An eye-safe transportable lidar system was developed by Aerospace for the specific purpose of mapping fugitive dust clouds. The system provides lidar dust data mapped onto Google Earth images of the surveyed site in real-time, allowing the operator to visualize the dust emission and its location relative to specific plant facilities. The real-time nature of the data provides a good understanding of the temporal behavior of the dust productions. In addition a co-aligned video camera records the visual aim-point of the lidar and any visual dust cloud present. This system was deployed to a site overlooking the Colton Portland Cement facility, approximately 1.5 km to the south. The lidar system was operated on three separate summer days over a two month time span. More than 20 hours of data were collected, resulting in thousands of stored lidar data files. The data showed persistent dust emissions from very specific locations on the plant site. The dust signals were very strong and localized, showing up almost entirely within the plant perimeter. The signals varied rapidly with time. Lidar horizontal scan patterns were established, similar to a radar beam scan, to monitor dust emissions over the course of hours. Results from the scans indicated the most prevalent locations on the plant facility for dust emissions. These locations are being correlated with specific plant activities to determine which processes are most responsible for producing dust. Lidar scans taken before and during plant operational hours verified that the dust production correlated with plant activity. The tests showed that lidar is an effective means of mapping fugitive dust emissions to plant locations and functions. It also demonstrated that lidar data can be used to track dust transport from sources to significant altitudes and away from the original source. One important application of these lidar capabilities is as a mitigation development and assessment tool. Current monitoring methods cannot pinpoint the sources of emissions within a plant. Identifying the most highly polluting operations within a plant allows air quality agencies to work with industry in developing mitigation strategies and allows assessment of the effectiveness of the mitigations. Information about the temporal and spatial nature of the emissions provided can also be employed to improve fugitive dust transport model assumptions. Lidar monitoring allows fugitive dust model inputs and outputs to be benchmarked against actual measurements. For example, on a relative scale, are the emission sources properly accounted by the model emission factors.

INTRODUCTION

Cement production facilities can be significant sources of fugitive dust emissions and PM pollution[1,2]. In addition to the inhalation health hazard due to its fine silica composition, depending upon the source of raw material and the fuel, cement dust can also contain significant amounts of heavy metals, including hexavalent chromium and mercury[3-5]. It is therefore critical that a detailed account of cement production processes and their contribution to the PM emission inventory be available. A detailed emission inventory provides a means for designing effective dust mitigation measures. Typically such inventories are compiled by models for the various plant processes which are not well benchmarked with measurements[6]. A high resolution spatial and temporal map of dust emission from an operating cement plant would allow correlation between specific plant operations and the dust which those operations produce. We report results of a pilot study to assess the efficacy of an eye-safe U.V. lidar for high resolution mapping of fugitive dust emission from a cement processing facility. The goal of the study was to determine if lidar could remotely provide detailed information on the correlation of specific process activities and dust emission at a level not possible by simple visual observation. Elastically scattered lidars have been used for many years to map various forms of aerosols and pollution[7], but not applied to cement plant emissions. So far as we know this is the first application of lidar to map fugitive dust emissions from a cement production facility. A small transportable UV elastic lidar was constructed and deployed to Colton, California to allow high-resolution three dimensional mapping of elastic returns from a local cement plant. Three days of data were recorded in various scan configurations from approximately 2 km distance. A co-boresighted video camera allowed visualization of the scanned features. Google Earth provided both a pointing aid as well a data visualization tool.

EXPERIMENTAL

Figure 1 shows a photograph of the mobile lidar system developed for this application and deployed to a ridge overlooking the Colton cement plant.

Figure 1 Lidar system overlooking cement plant

The lidar system consists of a 20Hz pulse repetition rate Nd:YAG laser (Spectra Physics Quanta Ray INDI), which is frequency tripled to 355 nm. The beam from the laser is expanded by a factor of ten and is directed collinear to the receiver telescope axis to the target. The receiver consists of a 15 cm aperture Newtonian telescope. Light from the secondary of the telescope is directed through an aperture and collimation optics through a narrow band (2angstrom FWHM) interference filter and is detected by a gated photomultiplier tube. Within the lidar shelter the laser is located on a shelf mounted to an optical table. The laser beam is routed around the table via high reflectivity dielectric mirrors. The receiver telescope mirrors are also mounted directly to the optical table for alignment stability. The optical filters and detectors are placed inside a light-tight box with an adjustable iris to control the field of view of the receiver. The scattered lidar signal is detected by a photomultiplier tube which converts photons to electrons with a gain of up to 80 db. The resulting transient lidar electrical waveform is digitized and recorded using a

100 MHz ADC (National Instruments). The interface software allows the operator to choose the averaging time. Both the receiver field-of-view (FOV) and the laser are directed together to the target by an azimuth/elevation mirror system which allows the FOV to be scanned over a full hemisphere. A co-bore-sighted video recorder with a wider field of view records the target scene and allows confirmation of pointing. As an indicator of the lidar sensitivity to particles, thin cirrus clouds have been detected easily with this system at ranges of more than 12km. The electrical supply for the lidar was a separate diesel generator. The system requires approximately 5KW of power to operate, including a rather large air conditioner window unit.

RESULTS AND DISCUSSION

Very strong lidar dust returns were measured localized over various portions of the cement plant despite them not being visible by eye or the video camera. An example of the lidar return is shown in Figure 2.
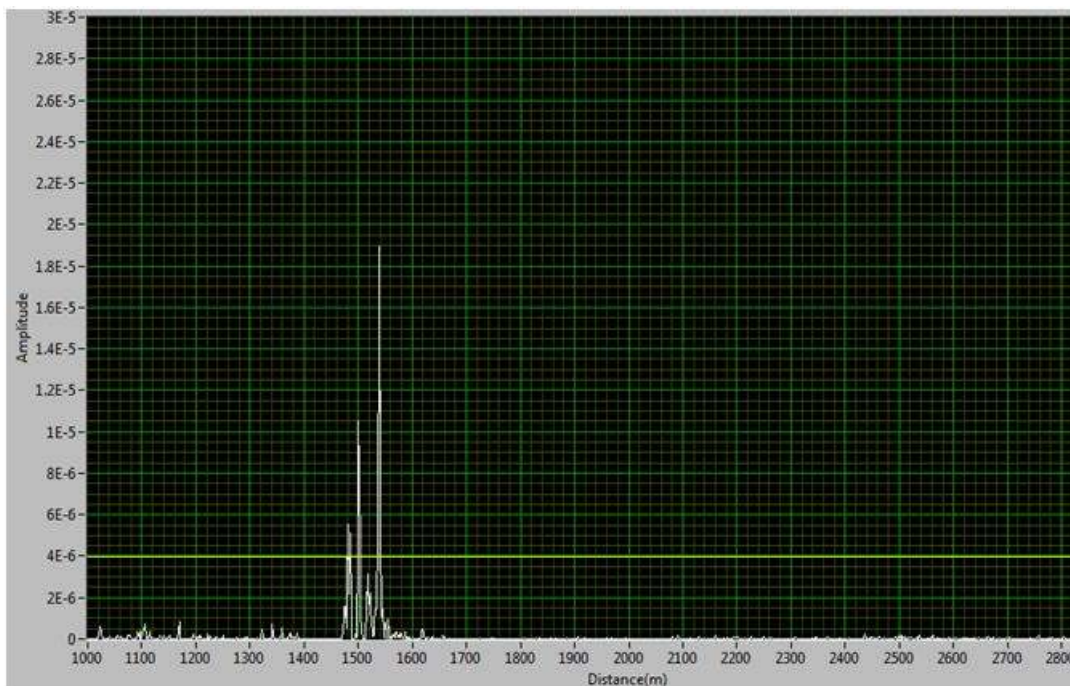

Figure 2 Lidar return from dust over cement plant. Signal is corrected for range and molecular scattering. The vertical axis is scattered intensity in arbitrary units; the horizontal axis is range from lidar position. Sharp peaks are sub-visual dust clouds. The horizontal line is a threshold setting used to determine the frequency of dust emission from locations during lidar scans.

The x-axis is range (distance) and the y-axis is signal intensity. The signal has been range and background corrected.   The general background consists of signals from scattered sun light, molecular scattering, and scattering from general ambient particulates, and scattering of the laser from the pointing mirror surfaces. These are eliminated by scanning the FOV away from the

4

cement plant and acquiring a background that can be subtracted. Scattering of the laser from nearby surfaces and ambient particulates and molecules, which is so strong it can saturate the detector and produce signal induced noise, is significantly reduced by gating the gain on the photomultiplier tube off for nearly one km worth of time. Therefore no signals are recorded or considered at distances less than 1km. The dust signals from the cement plant are easily identifiable based upon their strength and localized nature. Some of the widths of the plumes recorded are at the spatial resolution of the system, approximately 10m. The temporal behavior of the dust plumes was significant at even short durations, showing large changes within seconds or less. Typical would be the abrupt appearance of an intense localized signal which diminished rapidly and spread in spatial extent, as would be expected for dispersion of a dust plume. In most observations the prevailing wind was from west to east (see Figure 3) and only a small component of the wind was in the direction of the laser beam. We did observe a small general drift of the dust plume signals with time away from the lidar in the north east direction due to this small wind component.

Various scan configurations were implemented to derive a visualization of the dust emission behavior over the plant area. For example one scan pattern consisted of a horizontal scan 50 m above the highest object in the plant, covering repeatedly an angular area of 54 degrees in steps of 1 degree. This pattern is indicated in yellow shading in Figure 3.
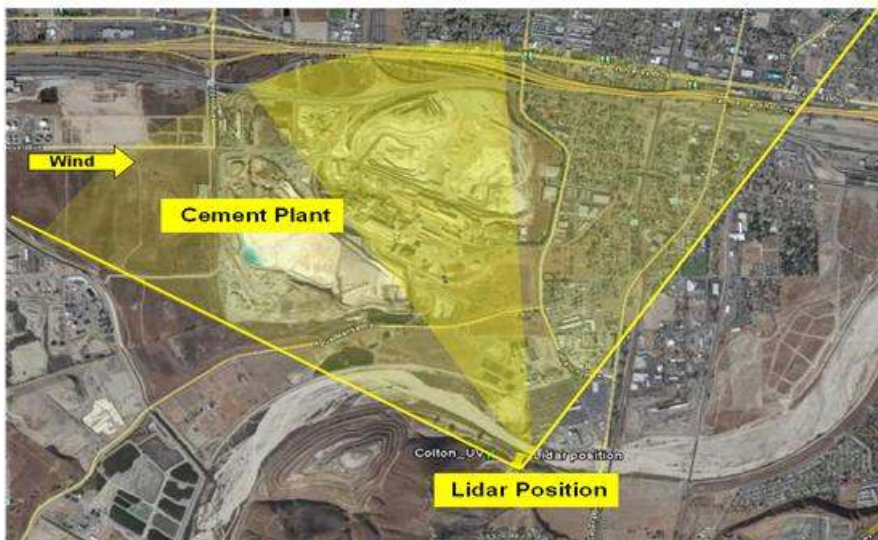

Figure 3 Google Earth image of cement plant and surroundings with lidar azimuthal scan patterns overlaid in yellow.

Narrower scan areas were also implemented at smaller angular step sizes of .25 degrees shown in darker yellow. For each step the signal was averaged for 1 to 2 seconds. Continuous repeating scans were taken in essentially autonomous operation for several hours. The scan data was processed and time averaged to provide areas of maximum dust signal and also areas of most frequent dust production. The frequency plots were developed by setting a threshold in the

processed data whereby if the signal crossed the threshold it was counted as a dust event during a scan. The position of the event was recorded and the number of events per position was tallied for the duration of the scanning. Figure 4 shows the results of a 1 hour and 50 minutes repetitive scan overlaid on a Google Earth image of the cement plant.
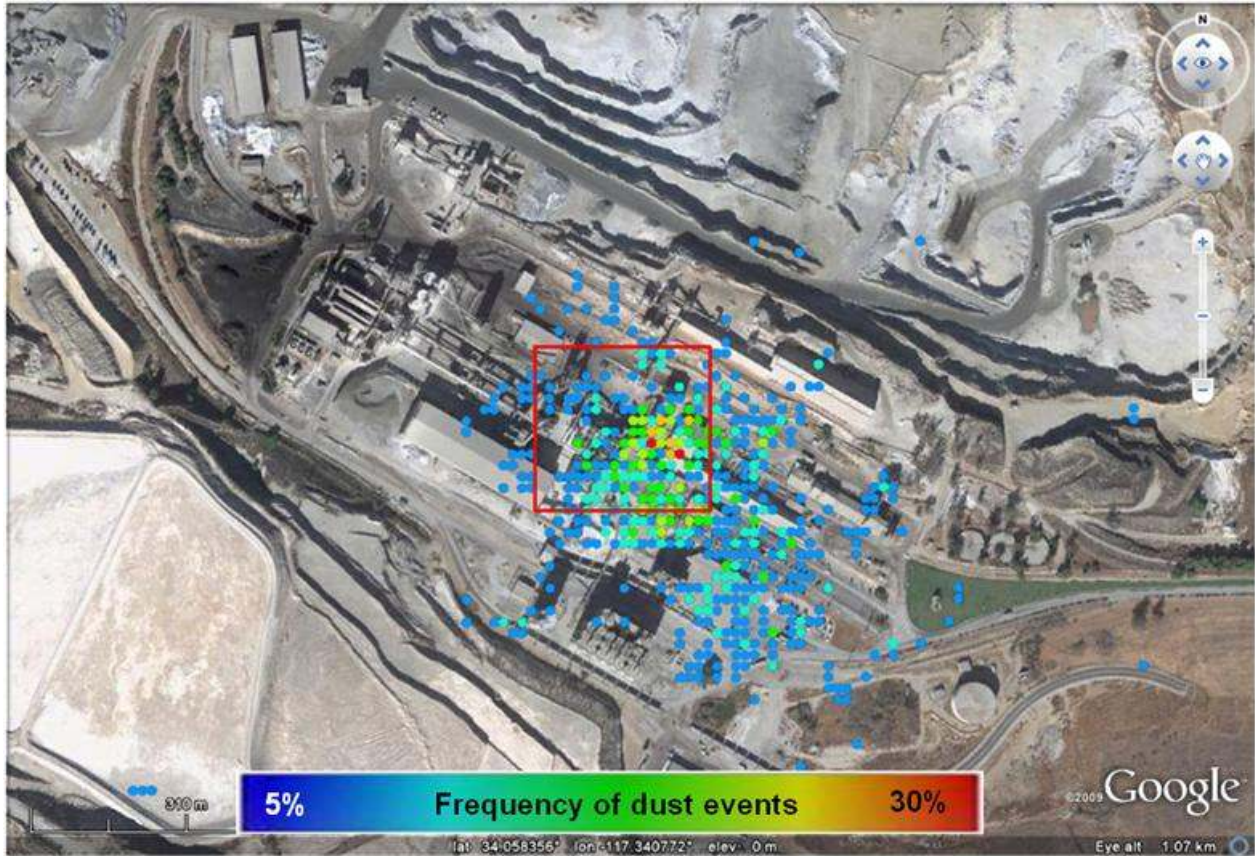

Figure 4 Google Earth image of cement plant overlaid with lidar data showing map of frequency of dust plume detections during a 1hour and 50 min repetitive scan.

Figure 4 represents the aggregation of data from 19 successive scans, each one taking a bit less than six minutes to complete. While a quantitative picture of how much dust is being detected by the lidar in terms of particle mass per air volume is not determined, if one assumes over the plant area that the size distribution and composition of the dust does not change appreciably, then relative intensity changes in the lidar signal correlate with dust concentration changes. That is, we assume stronger lidar signals correlate to larger dust concentrations. An example of lidar dust return intensity data integrated over an approximately 90 minute scan time is shown in Figure 5. The typical time evolution of the lidar signal intensity over the cement plant can be found in the APPENDIX, along with a detailed discussion on the challenges associated with quantifying dust concentrations from single color elastic scattering lidar measurements.
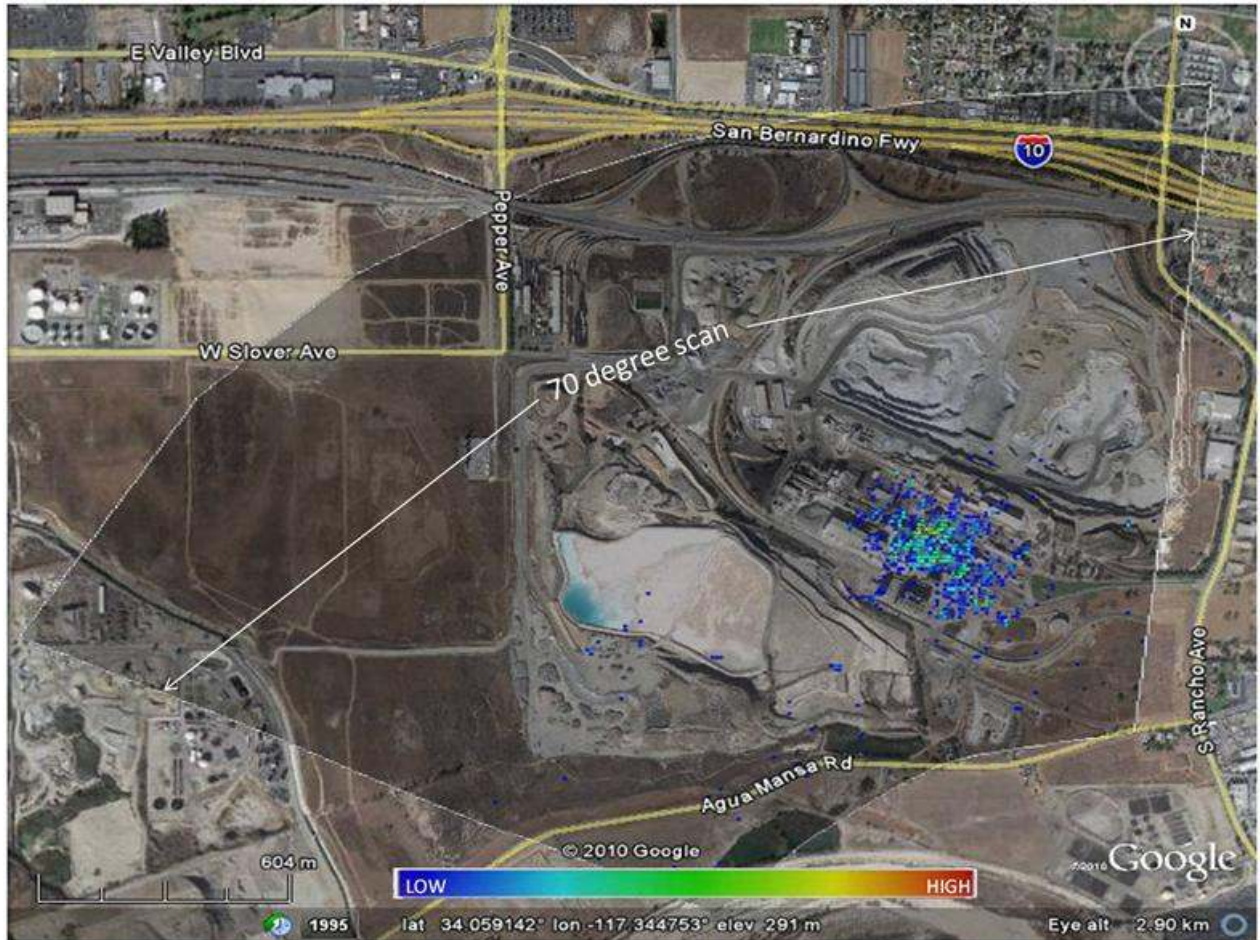
Figure 5 Google Earth image showing intensity of lidar returns integrated over an approximately 90 minute scan time. The extent of the azimuthal field of the scan is 70 degrees as indicated on the figure. Nearly all of the dust returns came from a small region of the scan localized over the plant building structures and silos. The lidar would cover the 70 degree field of regard in approximately 5 minutes and then reverse direction.

Vertical scans were also conducted to understand the transport nature of the emissions. Elevated columns of dust were common as shown in Figure 6. In this scan dust was observed as high as 194 m above ground level.
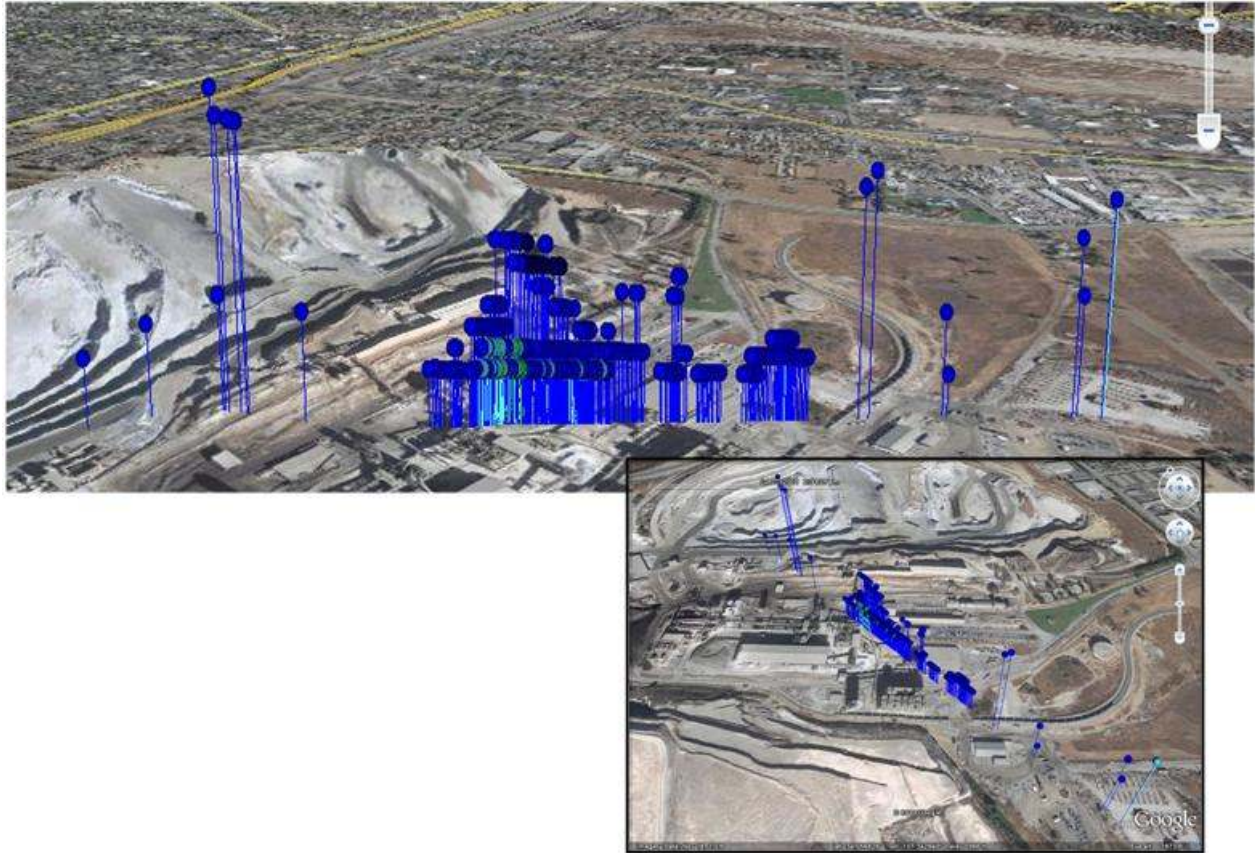
7

Figure 6 Google Earth image of cement plant overlaid with lidar data showing map of dust plume detections during vertical scan of plant.

The lidar results clearly indicate the areas of maximum dust emission. Simply by pinpointing these emission "hot spots" within a plant allows correlation between the emission and the production processes which are occurring at that location. Figure 7 shows another Google image of the cement plant with the various cement production processes located within the red circles on the map.
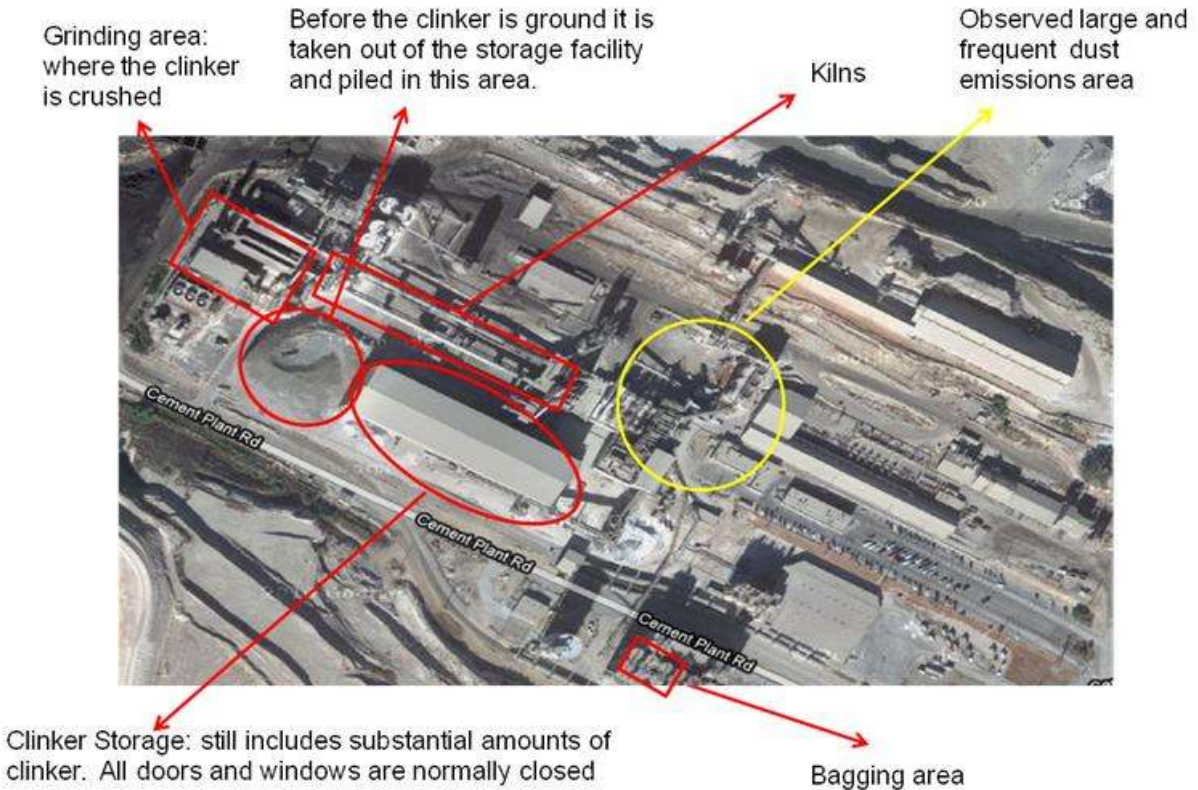
Figure 7 Google Earth image showing various cement production process locations outlined in red. The yellow outlined area indicates the area of most frequent and most intense dust observations during the lidar scanning. The production areas were identified by SCAQMD personnel.

The areas that were observed to be the most active dust producers did not correlate to any of the production areas circled in red. The lidar monitor data makes it very obvious what portion of the plant is producing dust and this can now be checked by local inspectors to see what process is indeed responsible. The lidar data also correlated emissions with plant operating hours. The lidar results shown in Figure 8 clearly demonstrate the increase in emissions as operations in the plant begin in the morning. Note that the cement kiln was not operating during the LIDAR observation periods.

7:15am~7:30am   7:30am~7:45am   7:45am~8:00am

Figure 8 Google Earth image showing correlation of emissions with plant operation schedule.

Results of the study demonstrated clearly the sensitivity of UV elastic lidar to sub-visual dust emissions and the spatial and temporal behavior of those emissions. Good correlations with process facilities and process activities could be derived from the lidar data.

CONCLUSIONS

This study demonstrated the ability of an eye-safe UV scanning lidar system to precisely map in three dimensions the fugitive dust emissions from an active cement plant. In addition, lidar was proven capable of characterizing the temporal behavior of the dust plumes as well as the horizontal and vertical transport of the dust. Sub-visual levels of dust emissions were easily detected with the lidar system. Additional work needs to be done if a quantitative value for the dust emissions is of interest. Good correlations to lidar dust signals and plant operations schedules were observed. Specific areas of the cement plant were repeatedly observed by lidar scans to produce the most dust most often and it remains to be determined exactly to which process this area corresponds. The data indicates that lidar could be highly useful as a means of identifying relative dust emission sources and transport from cement plants or other dust raising operations We are hopeful that these measurements can be extended to other operations and the data can be used to improve air quality, fugitive dust emission detection and mitigation efforts.

ACKNOWLEDGEMENTS

All trademarks, service marks, and trade names are the property of their respective owners.

APPENDIX A

Prospects for Quantitative Dust Measurements using Lidar

While single color elastic scattering lidar is an excellent tool for mapping dust plumes and their transport in three dimensions, it is not a trivial extension to make those measurements quantitative. That is it is difficult to accurately measure dust concentrations, either particles per volume or mass per volume, with single color lidar. The reason for this has to do with the fact that the amount of light scattered by a dust cloud depends upon a number of dust parameters which are generally not known and may not constant across a search area. The general lidar equation (1) governs the backscattered signal power measured by an elastic lidar system.

(1) $\quad P(R, \lambda) = (E/h\nu)(A/4\pi R^2)T_0\beta(R\ \lambda,)L\ \exp[-2\int_0^R \alpha(R')dR']$

Where P is the received signal power at the detector, E is the laser pulse energy, $h\nu$ is the scattered photon energy, A is the effective receiver area, T_0 is the transmission of the receiver optics, $\beta(R)$ is the backscattering coefficient at range R, L is the range interval, and α is the extinction coefficient. $\beta(R, \lambda)$ is the volumetric backscatter coefficient given by

(2) $\quad \beta(R,\lambda) = \beta mol(R,\lambda) + \beta aer(R,\lambda)$,

where the first term $\beta mol(R,\lambda)$ represents scattering by molecules and the second term, $\beta aer(R,\lambda)$ scattering by aerosols such as dust. The molecular scattering or Rayleigh scattering basically scales with air density. For horizontal paths such as used in this study it is a constant. The back-scattering coefficient for aerosols however is given by

(3) $\quad \beta aer(R,\lambda) = \Sigma_I\ n_i\frac{d\sigma(\lambda)}{d\Omega}$

Where $d\sigma_i(\lambda)/d\Omega$ is the differential backscattering cross-section of a single particle of species i and n_i is the number density of that particle species. This cross section is dependent upon a number of aerosol parameters such as size, shape, and index of refraction which are generally not known. And of course a dust cloud is not made up of a single type of particle but of an ensemble of sizes, shapes and compositions. Mie theory describes the light scattering from a spherical particle. Figure A-1 shows the results of a Mie scattering calculation for spherical water droplets with a prescribed size distribution. In this case the size distribution is a bimodal one with a small particle mean diameter of 0.1 microns and a large particle mean size of 1.0 microns. The hypothetical distributions are shown in the upper right corner of the figure. The plot shows the scattered power as a function of angle with respect to the incident angle of illumination. 180 degrees represents the backscattered intensity relevant to backscatter lidar signals. The plot in Figure A-2 is the same as Figure A-1 except the particle size distributions have been changed to include fewer small particles and more large ones. The plot again shows the scattered intensity

but the value for backscattered intensity is now 100 times larger than for the first distribution. This illustrates how sensitive the backscattered signal is to particle size distribution and how if that distribution is not well known it is so difficult to accurately extract particle concentration values from single color elastic lidar signals.
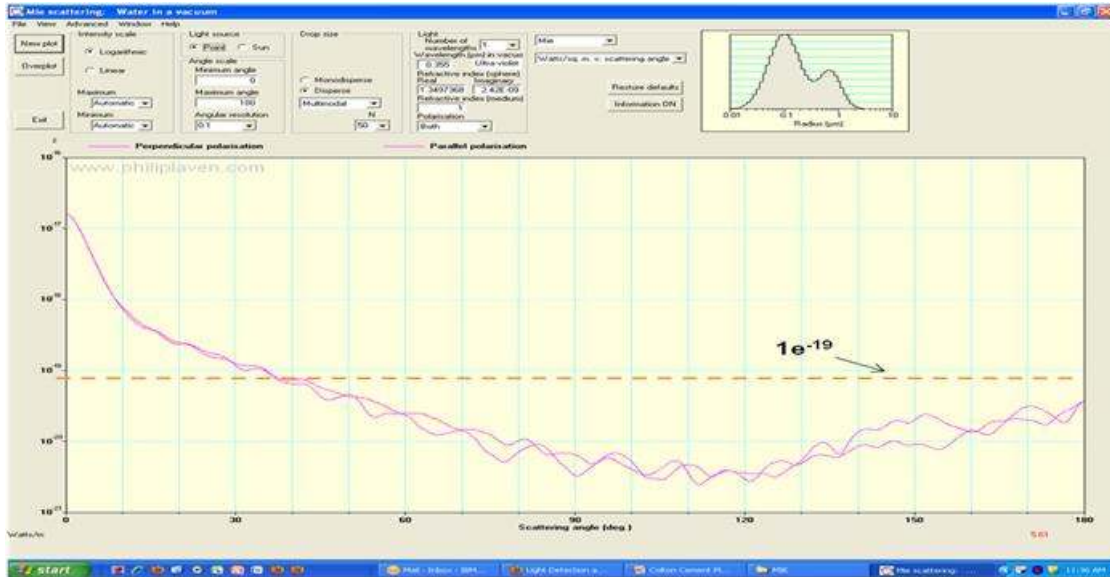

Figure A-1 Mie scattering calculation showing angle dependence of scattered power for particle distribution shown in upper right corner of figure. Dotted line indicates backscattered power.
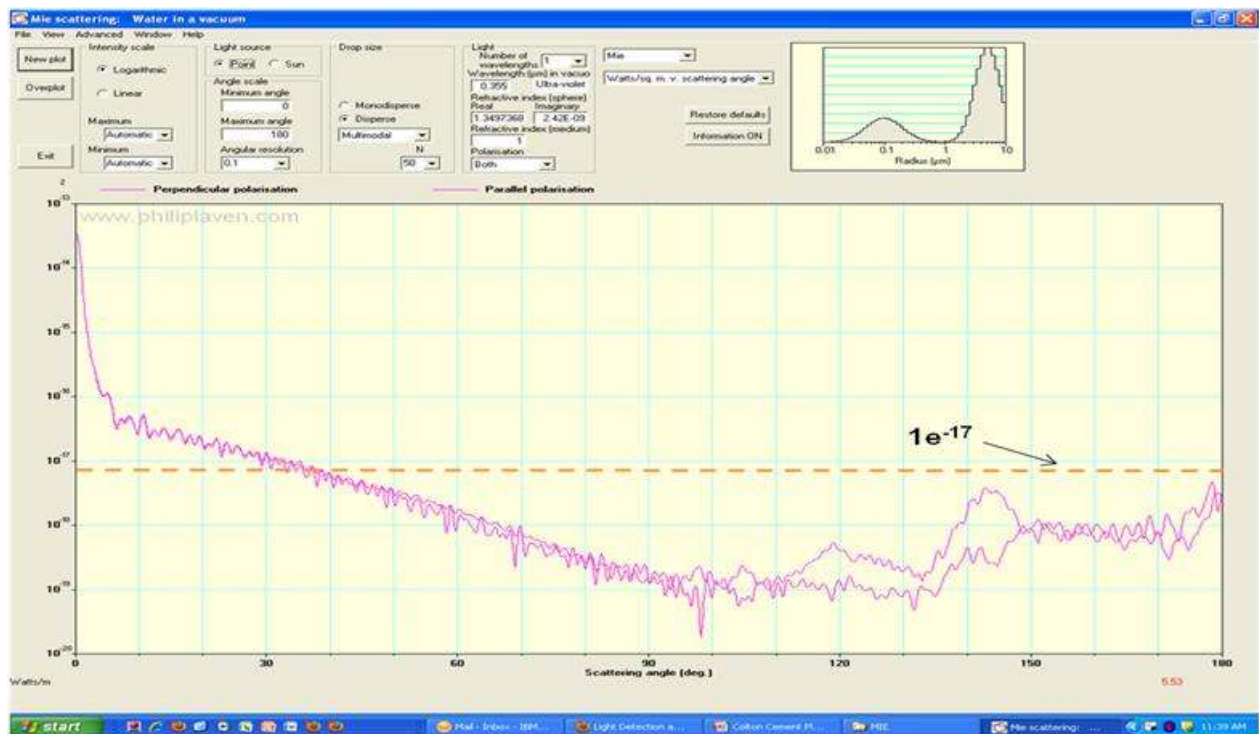
Figure A-2 Mie scattering calculation showing angle dependence of scattered power for particle distribution shown in upper right corner of figure. Dotted line indicates backscattered power.

There are possible methods to improve the level of quantitative information of dust clouds that can be extracted from elastic lidar signals. One can perform a type of calibration experiment where a plume of dust of known concentration and particle characteristics, including particle size distribution, composition and shape is artificially formed and then probed by the same lidar system to be used to map out the actual dust plumes. The signal could then be directly correlated to dust concentration with the assumption that other plumes in the region would consist of dust particles of roughly similar characteristics.   This is likely not a bad assumption for sites like the cement plant where the dust source should be fairly uniform across the plant. If on the other hand the dust source varies significantly from location to location, this calibration method would be less accurate.

Another possibility is to collect and analyze the dust of interest for size, shape, and composition using independent in-situ collection and measurement devices. Once the dust parameters have been established, scattering theory can be used to correlate backscattered intensity with dust concentration. Additionally a sample of the dust can be used to measure the light scattering properties at a specific wavelength, and this information used to predict lidar signals at the same wavelength and compared with the theoretical calculations[9].

14

Finally, lidar can easily measure optical extinction due to dust clouds quantitatively[8]. If optical extinction values can be related directly to dust concentrations by an independent means, lidar can provide a measure of dust concentration in a plume. For dust plumes such as encountered in this study, which are quite well defined and spatially distinct from the background scattering, the optical extinction can be measured by measuring the loss of scattered signal from one side of the plume to the other, as illustrated in Figure A-3.
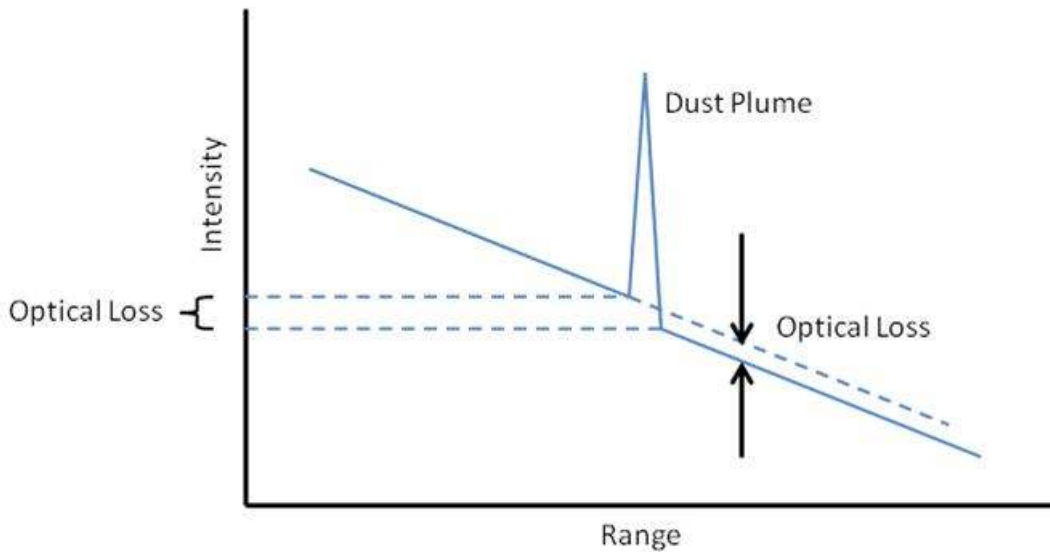

Figure A-3 Schematic representation of lidar backscattered signal through an optically thin, spatially confined dust plume. Optical loss is due to dust plume extinction.

Figure A-4 shows actual lidar data through an optically thin, spatially confined plume. The before section shows a decreasing background due to background scattering. The background is decreasing approximately exponentially due to the background extinction by mostly air molecules. After the plume, the background again is due to mainly molecular scattering and is decreasing with range. However the discontinuity in the two background levels is due to extinction through the plume. This is the measurement of interest. The vertical scale of this figure is expanded in Figure A-5 and the plume scattering is removed to emphasize the background discontinuity. The dotted horizontal lines indicate the magnitude of the optical extinction or loss due to the plume. This represents double the actual extinction due to the round trip of the lidar photons through the plume.
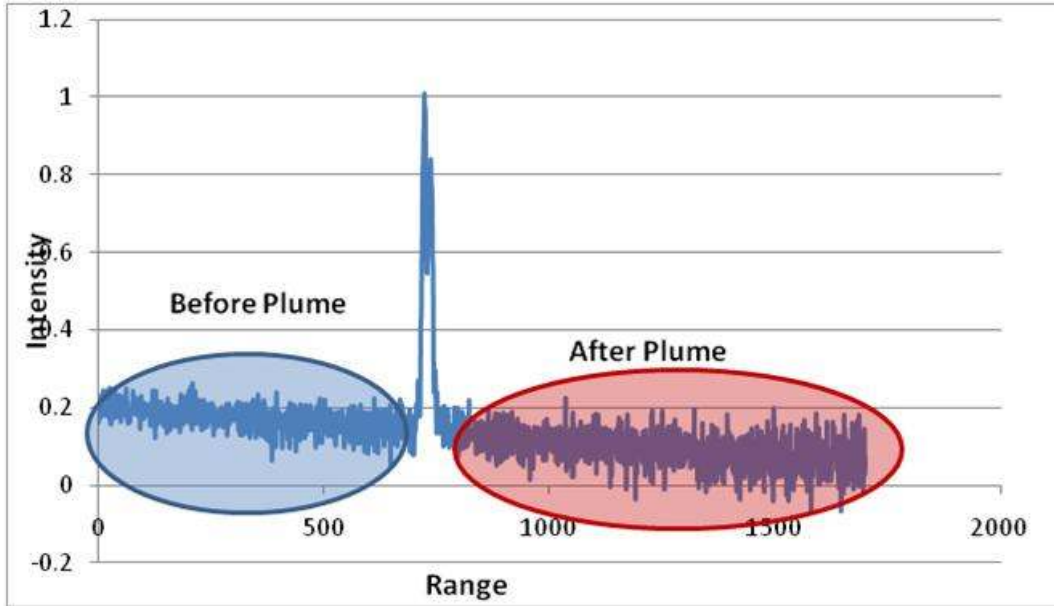
15

Figure A-4 Actual lidar data through a thin plume showing methodology for measuring optical extinction by plume.
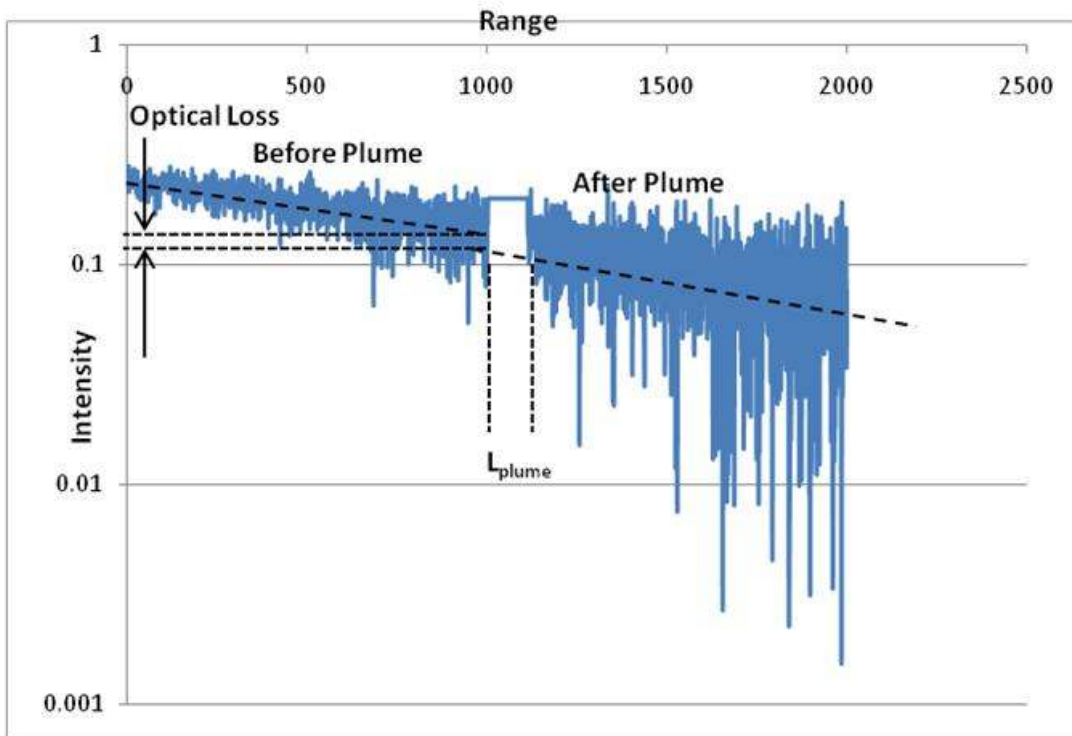

Figure A-5 Data expanded from Figure A-4 showing extraction of optical extinction due to traversal of plume. Actual plume data has been removed to allow scale expansion of baseline to highlight optical loss through plume.

16

Again, starting with the lidar equation (1)

$P(R, \lambda) = (E/h\nu)(A/4\pi R^2)T_0\beta(R\,\lambda,)L\,exp[-2\int_0^R \alpha(R')dR']$ and rearranging to focus on the extinction portion we have

(4) $\quad P = K\beta(R\,\lambda,)exp[-2\int_0^R \alpha(R')dR']$

where K is a factor containing terms independent of α and β.

In the "Before Plume" region the received power is denoted by

(5) $\quad P_{before} = K\beta(R\,\lambda,)exp[-2\int\alpha_{b,amb}(R')dR']$

Where $\alpha_{b,amb}(R')$ is the extinction caused by the horizontal path prior to the dust plume, due to the background scattering and absorption. Once the lidar beam propagates through the dust plume it experiences additional extinction due to the dust particles. Therefore once the beam exits the plume the plume must not be optically thick for these measurements to be obtained, which is very often the situation, the lidar beam has lost power due to the dust extinction and the ambient background scattering signal on the far side of the plume is reduced from the value it would have if the plume were not present. The amount of reduction of the background scattering signal is a measure of the plume extinction. The expression for the received lidar signal on the far side of the plume is given by

(6) $\quad P_{after} = K\beta(R\,\lambda,)exp[-2\int\alpha_{b,amb}(R')dR' - 2<\alpha_{plume}>L_{plume}]$

Where $<\alpha_{plume}>$ is an average extinction coefficient within the dust plume and L_{plume} is the distance through the plume. If Eq. (5) is divided by Eq. (6) we have

(7) $\quad (P_{before}/\,P_{after}) = exp(-2<\alpha_{plume}>L_{plume}$

Therefore the ratio of the return signal powers just before and just after the dust plume region provides a measure of the average extinction of the dust plume at the lidar wavelength. The above assumes that the ambient or background extinction is not changing before and after the dust plume. That is the plume is localized. This is the case for all of the measurements that were made at the cement plant location. In all cases the plumes were highly localized and the background scattering relatively constant.

In order to correlate plume extinction with plume particle density additional calibration, similar to that noted before for scattering signal calibration would need to be carried out. Measuring extinction from a dust sample at the appropriate wavelength is likely easier and more accurate than trying to measure the backscattered signal intensity as a function of dust concentration.

APPENDIX B

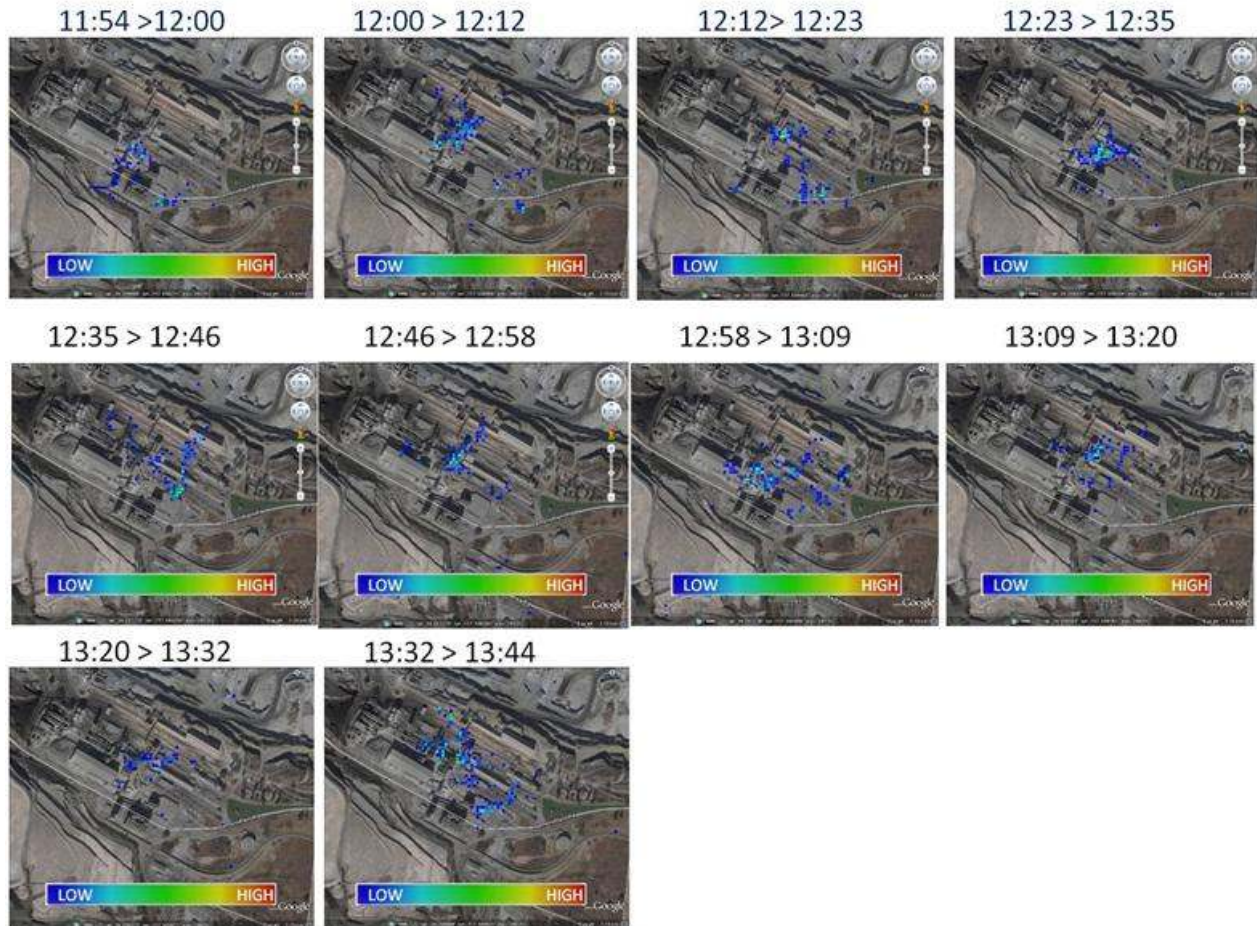## Typical Time Evolution of Lidar Signal Intensity

Figure A-6 Time series of plots showing the intensity of lidar dust returns and how the pattern of emissions changes over time. The intensity of the lidar returns is color coded where blue is low end of the range to red which is the high end. No color indicates no lidar return was collected from that location. Each of the plots is an integration of intensity of lidar dust returns over an approximately 10 minute time span. Each plot is contiguous in time to the plot before and after in the series. The time of the data acquisition in local time for each plot is indicated above each plot. The series show that while the dust emission sources move about the plant somewhat, the pattern is fairly localized and consistent. This series of intensity plot "snapshots" provide another means to look at the frequency of dust emission as a function of location.
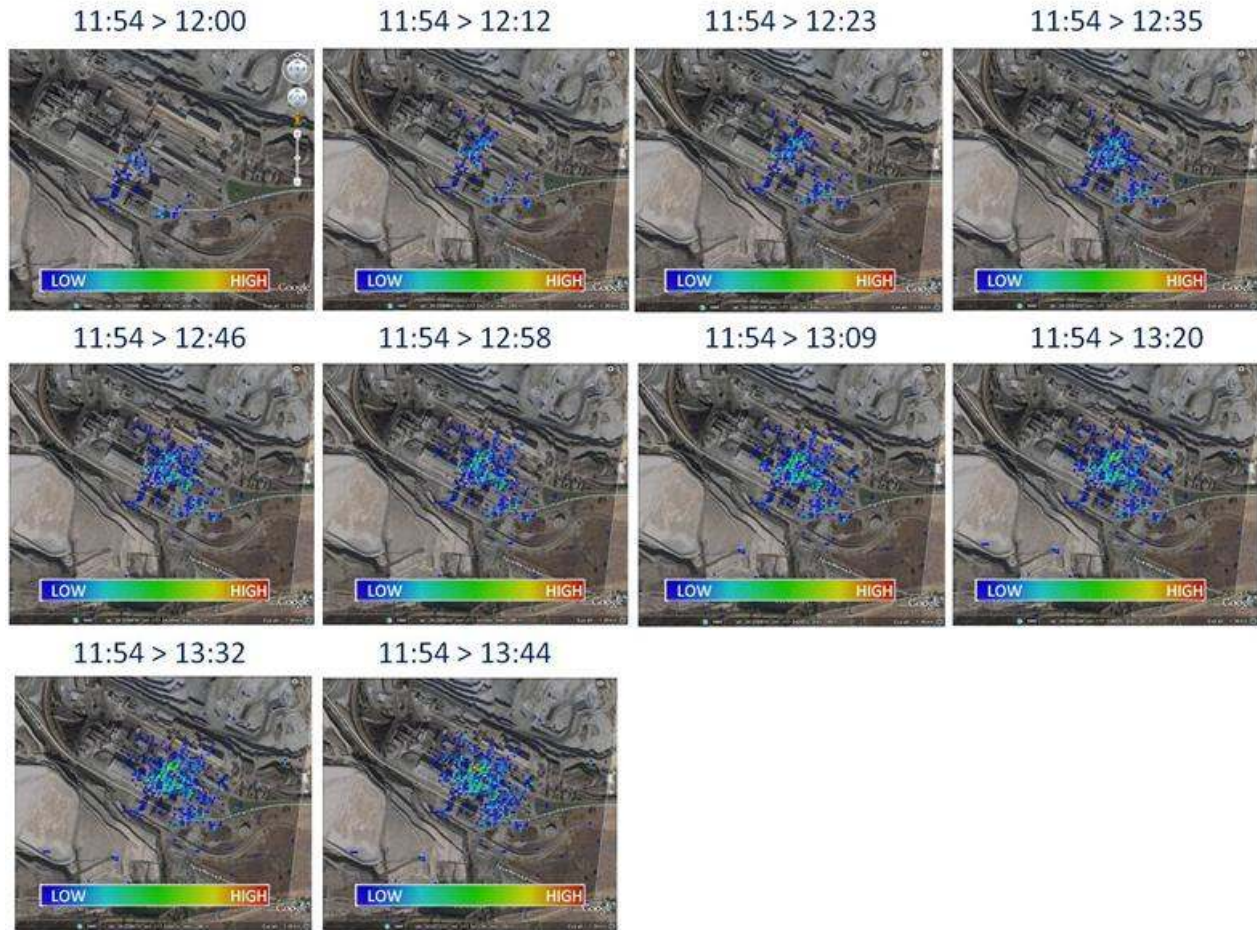
Figure A-7 Series of plots indicating the integral on the lidar dust signal intensity as a function of time and location. This data is the same data as shown in figure A-6 except that the lidar intensity is integrated from the time the scan was initiated until the time indicated above each plot. So the first panel represents the integral of intensity over six minutes, the second panel the integral of intensity over 18 minutes etc. The figure is meant to show the accumulation of dust emission area over time.

REFERENCES

1. Technical Background Document for the Notice of Data Availability on Cement Kiln Dust, "Human Health and Environmental Risk Assessment, in Support of the Regulatory Determination on Cement Kiln Dust". U.S. Environmental Protection Agency, 1994. Office of Solid Waste, Washington, D.C., August, 1994.

2. Technical Background Document: "Population Risks from Indirect Exposure Pathways, and Population Effects from Exposure to Airborne Particles from Cement Kiln Dust Waste". U.S. Environmental Protection Agency, 1997. Office of Solid Waste, Washington, D.C., June, 1997.

3. "AQMD detects high levels of hexavalent chromium, cites Inland cement plant", David Danelski and Gregor McGavin, The Press-Enterprise, April 15, 2008
http://www.pe.com/localnews/inland/stories/PE_News_Local_D_cement16.3b90d46.html

4. Hills, Linda M and Johansen, Vagn C., "Hexavalent Chromium in Cement Manufacturing: Literature Review", SN2983, Portland Cement Association, Skokie, Illinois, USA, 2007

5. "EPA requires cleanup of mercury from cement plants", Renee Schoof, McClatchy NewpapersAug. 9th 2010 http://www.mcclatchydc.com/2010/08/09/98878/epa-requires-cleanup-of-mercury.html?utm_source=twitterfeed&utm_medium=twitter&utm_term=news

6. "Impact of fugitive dust emissions from cement plants on nearby communities", Sabah A. Abdul-Wahab, Ecological Modelling
Volume 195, Issues 3-4, 15 June 2006, Pages 338-348

7. "Lidar Applied in Atmospheric Pollution Monitoring", K. Fredriksson, B. Galle, K. Nystrom, and S. Svanberg, Applied Optics 18, No. **17** / **1,** 3000 1979"

8. "Lidar for Remote Measurement of Ozone in the Exhaust Plumes of Launch Vehicles", Jerry A. Gelbwachs, Applied Optics 35, 2630 (1996)

9. "Emission Inventories - Applying New Technologies", Dennis Fitz, David Pankratz, Russell Philbrick and Guangkun Li,12th International Emission Inventory Conference Papers and Presentations San Diego, April 29 - May 1, 2003